DELPHI Collaboration DELPHI 2000-003 PHYS 846
12 January, 2000

The Measurement of the Cross Section and Forward–Backward Asymmetry for $e^+e^- \to \mu^+\mu^-(\gamma)$ at LEP2

A. Behrmann, T. Burgsmüller
University of Wuppertal
J.F. Libby, G.W. Morton
University of Oxford

Abstract

This note presents the DELPHI analyses of the $e^+e^- \to \mu^+\mu^-(\gamma)$ process at LEP2 centre–of–mass energies ($\sqrt{s}$). The data taken between the autumn of 1995 and 1998 have been used. The cross section ($\sigma^{\mu\mu}$) and forward–backward asymmetry ($A_{\rm FB}^{\mu\mu}$) have been evaluated for two ranges of effective invariant mass ($\sqrt{s'}$): $\sqrt{s'} > 75$ GeV and $\sqrt{s'}/\sqrt{s} > 0.85$. The first range of $\sqrt{s'}$ includes the radiative return events to the Z^0. The second range is a subset which contain the non–radiative events with a $\sqrt{s'} \sim \sqrt{s}$; these events are most sensitive to new physics contributions to the process. In addition to the cross–section and forward–backward asymmetry, the differential cross–sections are given for the 1997 and 1998 data sets. This note also contains a discussion of the systematic uncertainties on $\sigma^{\mu\mu}$ and $A_{\rm FB}^{\mu\mu}$.

1 Introduction

This note will describe the measurement of the $e^+e^- \rightarrow \mu^+\mu^-(\gamma)$ cross section ($\sigma^{\mu\mu}$) and the forward–backward asymmetry ($A_{\rm FB}^{\mu\mu}$) at all LEP2 energies from 1995 to 1998. In addition, the differential cross sections will be presented for the data taken at 183 GeV and 189 GeV during 1997 and 1998. The results given here have been presented in several publications [1, 2], alongside other $e^+e^- \rightarrow f\bar{f}$ results .

LEP2 has allowed the study of the $e^+e^- \rightarrow f\bar{f}$ at energies above the Z^0 resonance for the first time. The measurement of fermion pair production at LEP2 has led to the setting of limits on the parameters of several new physics processes: contact interactions, $\not{R}$ supersymmetry, Z' bosons and gravity interactions. Further details of these new physics processes can be found in [1] and [3] and the references therein.

The layout of the note is as follows. Initially, the signal and background processes are described in Section 2. Section 3 will define the data samples used and give the corresponding luminosities and mean centre–of–mass energies ($\sqrt{s}$). This will be followed by a description of the majority of the $e^+e^- \rightarrow \mu^+\mu^-(\gamma)$ selection criteria and the muon identification algorithm in Section 4. The importance and evaluation of the effective invariant mass ($\sqrt{s'}$) of the muon pair will then be described in Section 5. A brief description of the determination of the selection efficiency from both data and simulation will then be given in Section 6. In Section 7 the results will be presented and compared to the Standard Model predictions. A full description of the systematic uncertainties on both $\sigma^{\mu\mu}$ and $A_{\rm FB}^{\mu\mu}$ will also be presented in Section 7.

The analysis presented here has been performed independently by groups from both Oxford and Wuppertal. The analysis methods used are very similar and the following description will only distinguish between them where there is a significant difference.

2 The signal topology and backgrounds

The distinctive topology of a muon pair event is two well isolated and oppositely charged tracks, with high momentum. Furthermore, events with this topology will have the two fastest tracks (more than two charged tracks may be present in an event due to, for instance, conversions in the detector) with muon chamber hits as well as low energy depositions within the calorimeters. At energies above the Z^0 resonance approximately 50% of muon pair events observed contain significant Initial State Radiation (ISR) leading to the effective invariant mass of the muon pair ($\sqrt{s'}$) to be close to that of the Z^0. These radiative events normally have a significant acollinearity. Non–radiative events produced with a $\sqrt{s'} \sim \sqrt{s}$ do not have a significant acollinearity.

There are four significant sources of background to radiative and non–radiative events: $\tau^+\tau^-$, $e^+e^- \rightarrow e^+e^-\mu^+\mu^-$, fully–leptonic W^+W^- decays and cosmic ray muons. All these processes can yield a final state identical to a muon pair event within the detector. The process $e^+e^- \rightarrow e^+e^-\mu^+\mu^-$ can be produced by two–photon events or by neutral current processes involving one or two Z^0 bosons. The neutral current processes were found to contribute a negligible background and are subsequently neglected. In Section 4 the selection criteria which discriminate against each background will be indicated.

Year	Energy (GeV)	Integrated Luminosity (pb^{-1})
1995	130.2	$2.867 \pm 0.010(stat.) \pm 0.016(syst.)$
	136.2	$2.996 \pm 0.011(stat.) \pm 0.017(syst.)$
1996	161.3	$9.514 \pm 0.037(stat.) \pm 0.053(syst.)$
	172.1	$10.166 \pm 0.046(stat.) \pm 0.057(syst.)$
1997	182.7	$51.573 \pm 0.087(stat.) \pm 0.532(syst.)$
1998	188.6	$156.345 \pm 0.165(stat.) \pm 0.874(syst.)$

Table 1: The integrated luminosity after run selection and the luminosity weighted average energies for all periods of LEP2 running during 1995-1998.

3 The Data Set

The run selection removed runs in which the TPC had an efficiency $< 90\%$ or the MUB or MUF was known to be operating badly. Lists of the bad MUC runs were provided by the groups operating the individual sub–detector. For the cross–section analysis a run without a corresponding luminosity measurement was also excluded; these runs were included in the forward–backward asymmetry analysis.

The integrated luminosities used in the different years analysed are given in Table 1. Table 1 also gives the luminosity weighted mean centre–of–mass energies at which LEP ran in the different years.

4 The Event Selection

The event selection procedure is described in three parts: the basic topological and kinematic criteria, the muon identification and the cosmic ray rejection.

4.1 Basic Selection Criteria

The basic selection criteria fall into two classes: topological and kinematic. The cuts used are summarised in Table 2. The cuts and their motivation are given below.

4.1.1 The Charged Multiplicity (N_{ch})

A cut on N_{ch} was motivated by the basic two prong topology of a muon pair. The upper cut, requiring 7 charged tracks or less to have been reconstructed, removed hadronic events. The upper cut was not made at a lower value because the charged multiplicity of a true muon event can be increased by photon conversions or split tracks[1] .

[1] A split track is one where there are track elements from two detectors, i.e. the TPC and the muon chambers, that belong to one real track but are not associated by the track reconstruction algorithm

Topological	
Charged Multiplicity	$2 \leq \mathrm{N_{ch}} \leq 7$
Angular Acceptance	$20^\circ \leq \theta_{1,2} \leq 160^\circ$
Kinematic	
Track Momentum	$\|\mathbf{p_1}\| > 30$ GeV, $\|\mathbf{p_2}\| > 5$ GeV
Additional Charged Tracks	$\|\mathbf{p_3}\| < 5$ GeV if $\|\mathbf{p_1}\| < 0.9 E_{\mathrm{BEAM}}$ GeV

Table 2: The values of topological and kinematic cuts used in the basic selection

4.1.2 The Angular Acceptance

For the data taken from 1995 to 1997 an event was accepted only if the two highest momentum tracks had a polar angle, θ_1 and θ_2 respectively, within the acceptance 20°-160°. In this region tracking and trigger efficiency were known to be stable and uniform from LEP1 [4]. Ideally the acceptance should be opened further; however, the statistics for cross–checks between data and simulation, for isolated tracks with high–momentum, are limited in the forward region for these data sets. In 1998 the statistics were large enough to allow these studies to be performed; these are presented in [5]. Subsequently the acceptance was opened to 14°-166° for the 1998 analysis.

4.1.3 Momentum Cuts

Cuts on the momentum of both the first and second fastest track were made. These cuts were placed at $|\mathbf{p}_1| > 30$ GeV and $|\mathbf{p}_2| > 5$ GeV. As can be seen from Figure 1 this cut reduces the contamination from $\tau^+\tau^-$, two–photon and fully leptonic WW events. The cut was loose as the further cut placed on $\sqrt{s'}$ eliminated much of the background.

The generators used in Figure 1 were `KORALZ` [6] for $\mu^+\mu^-$ and $\tau^+\tau^-$ events, `EXCALIBUR` [7] for the $\mathrm{W^+W^-}$ events and `BDKRC` [8] for two photon events. These generators have been used in this note unless stated otherwise.

4.1.4 Rejection of Additional Charged Tracks

If there was a third charged track with $|\mathbf{p}_3|$ greater than 5 GeV the event was rejected. This was to reduce contamination from τ pair events. This cut was not applied if the fastest track had a momentum greater than 90% of the beam energy. Figure 1 shows that a muon with such a momentum was most likely to come from a muon pair event.

4.2 Muon Identification

Muon identification was performed individually on the two highest momentum tracks. The event was selected if both tracks had positive muon identification. Each track had to pass at least one of the following criteria:

- the number of MUC hits associated to a track was ≥ 1.
- the associated energy in the HCAL per layer was ≤ 5 GeV/$\sin^2\theta$ for $50^\circ < \theta < 130^\circ$ and ≤ 5 GeV outside this range. Some of the energy deposited was required to be in the two outer layers of the HCAL.

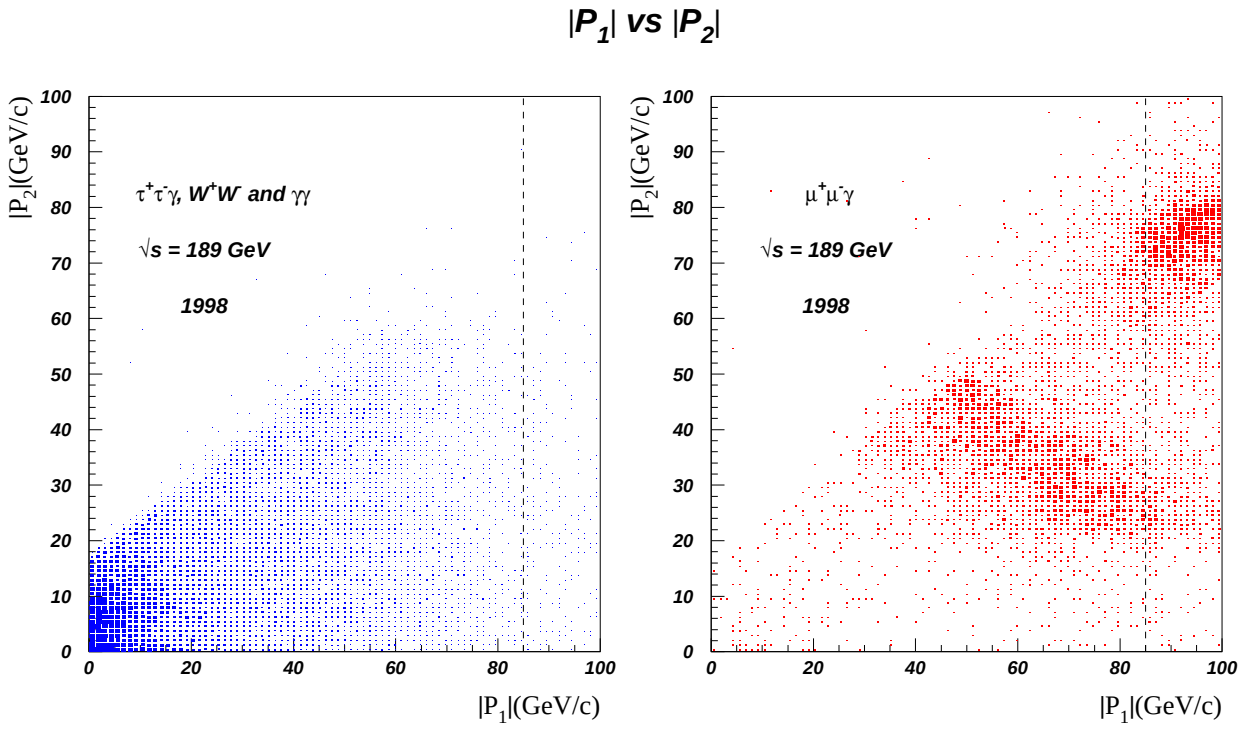

Figure 1: The momentum of the first ($|\mathbf{p}_1|$) and second ($|\mathbf{p}_2|$) fastest tracks are plotted against one another. The samples used are simulations at 189 GeV and are normalised to the effective luminosity of the $e^+e^- \to \mu^+\mu^-(\gamma)$ sample. The background processes (left–hand plot) can be seen to cluster at lower values of momenta than the signal process (right–hand plot). The line represents the value of $|\mathbf{p}_1|$ at which the cut on the momentum of additional charged tracks was no longer applied.

- the ECAL energy associated to the track was ≤ 1.5 GeV.

In addition, there were two vetoes on events in place. An event was rejected:

- if one of the fastest two tracks had an HCAL energy per layer greater than 5 GeV, with no associated muon chamber hits. This reduced the number of charged pions misidentified as muons.
- if there was an ECAL energy greater than 10 GeV associated to either of the two fastest tracks, with no muon chamber hits associated to either track. This veto removed tau pair events.

This muon identification algorithm was developed and rigorously tested during the analysis of LEP1 data [9, 4] and remains valid at LEP2 energies.

4.3 Cosmic Ray Rejection

Initially loose impact parameter cuts were applied to the preselected sample. This served as a preliminary cut for cosmic ray muon rejection as well as defining a volume in impact parameter space from which the contamination of cosmic ray muons into the muon pair

Track Type	$\lvert IP_{R\phi}\rvert$ (cm)	IP_z (cm)
VD	0.1	2.0
TPC/ID	1.0	2.0
Other	1.0	2.0

Table 3: The cuts placed on $|IP_{R\phi}|$ and the IP_z depending on which detectors were used to reconstruct the track.

sample may be estimated. This is described later. Tight impact parameter cuts were applied to reject cosmic ray muons. Figure 2 gives a distribution of $IP_{R\phi}$ values, with respect to the beamspot, for events that passed the basic selection cuts and the muon identification criteria. The points along the negative diagonal, away from the cluster at the origin, are cosmic events where the track was displaced from the nominal beam spot.

The cuts placed on $|IP_{R\phi}|$ depended on which tracking sub–detectors had participated in the reconstruction of the track. Events without associated hits in the vertex detector had much looser cuts than those with. The cuts used on both $|IP_{R\phi}|$ and IP_z are given in Table 3. The residual cosmic ray background was evaluated by using events that pass the IP_z cut but failed the $|IP_{R\phi}|$ cut. A distribution of such events is given in Figure 3. By extrapolating into the central region around the origin the cosmic background can be determined. The events which had one impact parameter greater 0.1 cm are events where one track was without associated VD hits.

5 The Evaluation of $\sqrt{s'}$

The value of $\sqrt{s'}$ is an important variable with respect to the measurement of $\sigma^{\mu\mu}$ and $A_{\rm FB}^{\mu\mu}$ because the sensitivity to new physics is greatest for events with a value of $\sqrt{s'}$ close to the collision energy of the beams, $\sqrt{s}$. Furthermore, it is an excellent discriminator between the signal and the background processes. Every increase in the LEP energy opens a previously unexplored kinematic region of $\mu^+\mu^-$ production in e^+e^- collisions. The radiative return events with a value of $\sqrt{s'}$ close to the mass of the Z^0 do not provide a good probe of new physics. However, the sample of low multiplicity $e^+e^- \to \mu^+\mu^-(\gamma)$ events are an ideal environment in which to study the radiative return process.

Therefore, the values of $\sigma^{\mu\mu}$ and $A_{\rm FB}^{\mu\mu}$ are evaluated for two different regions of $\sqrt{s'}$, at each value of $\sqrt{s}$: muon pair events with $\sqrt{s'} > 75$ GeV, which includes events with $\sqrt{s'} \approx M_Z$ and the subset of these events with $\sqrt{s'}/\sqrt{s} > 0.85$, which are most sensitive to physics beyond the Standard Model. The cut to select non–radiative events was placed at $\sqrt{s'}/\sqrt{s} > 0.85$ because it was found to yield a reasonable optimal value of the sensitivity to new physics considering the values of $\sqrt{s}$ at which LEP has run [10].

5.1 Methods of $\sqrt{s'}$ Calculation

The invariant mass of the muon pair is taken to be that of the two tracks identified as muons; no attempt has been made to incorporate Final State Radiation. Therefore, the

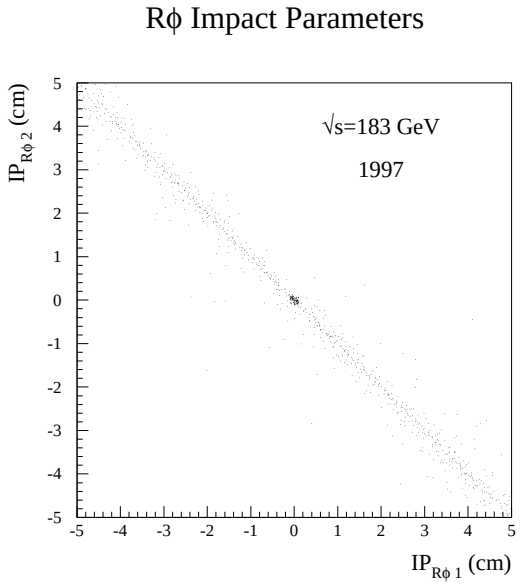

Figure 2: The impact parameter of the first (IP$_{R\phi 1}$) and the second (IP$_{R\phi 2}$) fastest tracks are plotted against one another. Only the events that pass the basic cuts and muon identification criteria were used. The cosmic muon events are those along the diagonal away from the nominal interaction region.

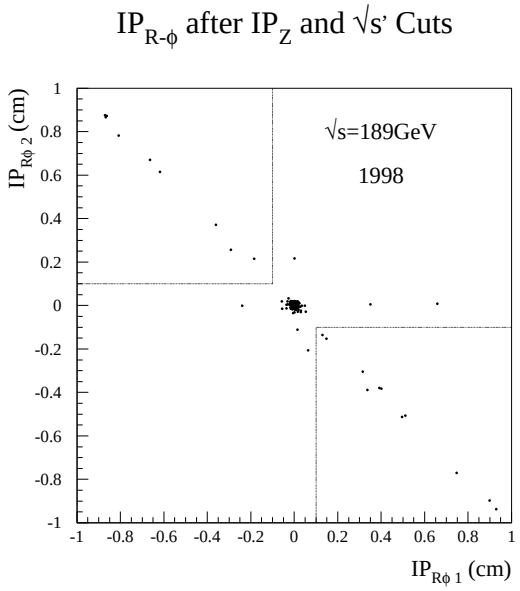

Figure 3: The impact parameter of the first (IP$_{R\phi 1}$) and the second (IP$_{R\phi 2}$) fastest tracks are plotted against one another after IP$_z$ cuts and a cut $\sqrt{s'} > 75$ GeV (the evaluation of $\sqrt{s'}$ is described in Section 5) had been placed. The events along the diagonal which are inside the boxes marked by the dashed line are used to extrapolate into the region around the origin to evaluate the cosmic background.

square of the effective invariant mass is defined to be:

$$s' = (E_{\mu^-} + E_{\mu^+})^2 - (\mathbf{p}_{\mu^-} + \mathbf{p}_{\mu^+})^2, \tag{1}$$

where $E_{\mu^\pm}$ and $\mathbf{p}_{\mu^\pm}$ are the energy and 3–momentum of the $\mu^\pm$ respectively. Neglecting the mass of the muon Equation 1 can be written as:

$$s' = (|\mathbf{p}_{\mu^-}| + |\mathbf{p}_{\mu^+}|)^2 - (\mathbf{p}_{\mu^-} + \mathbf{p}_{\mu^+})^2. \tag{2}$$

However, substituting the measured momentum of the muon pair in to Equation 2 to evaluate $\sqrt{s'}$ is not the ideal estimator. The resolution of $\sqrt{s'}$ may be improved upon by either the *angular method* or constrained fitting, both of which are described below. The resolution on $\sqrt{s'}$ using the measured track parameters, compared to these two methods, is given in Figure 4.

5.1.1 The Angular Method

The simplest alternative method to evaluate $\sqrt{s'}$ uses only the polar angles of the muon pair and $\sqrt{s}$; this is termed the *angular method*. If only one photon has been radiated, in a direction collinear to that of the beams, the muon pair event becomes a two–dimensional system as illustrated in Figure 5.

Using 4-momentum conservation, the energy of the photon, E_γ, can be written in terms of the polar angles of the muons and $\sqrt{s}$ alone:

$$E_\gamma = \frac{|\sin(\theta_{\mu^+} + \theta_{\mu^-})|\sqrt{s}}{\sin(\theta_{\mu^+}) + \sin(\theta_{\mu^-}) + |\sin(\theta_{\mu^+} + \theta_{\mu^-})|}, \tag{3}$$

where θ_{μ^+} and θ_{μ^-} are the μ^+ and μ^- polar angles respectively.

The application of four momentum conservation to any singly radiative muon pair event allows Equation 2 to be written in terms of $\sqrt{s}$ and E_γ alone:

$$s' = s - 2E_\gamma\sqrt{s}\,. \tag{4}$$

The substitution of the expression for E_γ, given in Equation 3, into Equation 4 gives $\sqrt{s'}$ in terms of the polar angles of the two muons and $\sqrt{s}$:

$$\sqrt{s'} = \left(\frac{\sin(\theta_{\mu^+}) + \sin(\theta_{\mu^-}) - |\sin(\theta_{\mu^+} + \theta_{\mu^-})|}{\sin(\theta_{\mu^+}) + \sin(\theta_{\mu^-}) + |\sin(\theta_{\mu^+} + \theta_{\mu^-})|}\right)^{\frac{1}{2}} \sqrt{s}\,. \tag{5}$$

This formula is precise for non–radiative events because in the limit of $\theta_{\text{acol}} \approx 0°$ ($\theta_{\mu^-} + \theta_{\mu^+} = 180°$) the formula reduces to $\sqrt{s'} = \sqrt{s}$. However, the *angular method* no longer gives a good approximation to $\sqrt{s'}$, for events in which either an ISR photon has been radiated with significant transverse momentum or, two or more photons have been radiated. Events with FSR, where the photon is emitted in a direction other than along the direction of the beampipe, are also not well described by this method.

It is important to note that a reconstructed cosmic ray has a value of $\theta_{\text{acol}} \approx 0°$, leading to a value of $\sqrt{s'}$ equal to $\sqrt{s}$ when applying the angular formula. This is not necessarily the case upon application of equation 1, where the $\sqrt{s'}$ value can be over the whole range of effective mass. Subsequently the cosmic contamination is increased in the interesting non–radiative class of events when the *angular method* is used. Therefore, it was desirable to find another method to determine the $\sqrt{s'}$ of the muon pair events.

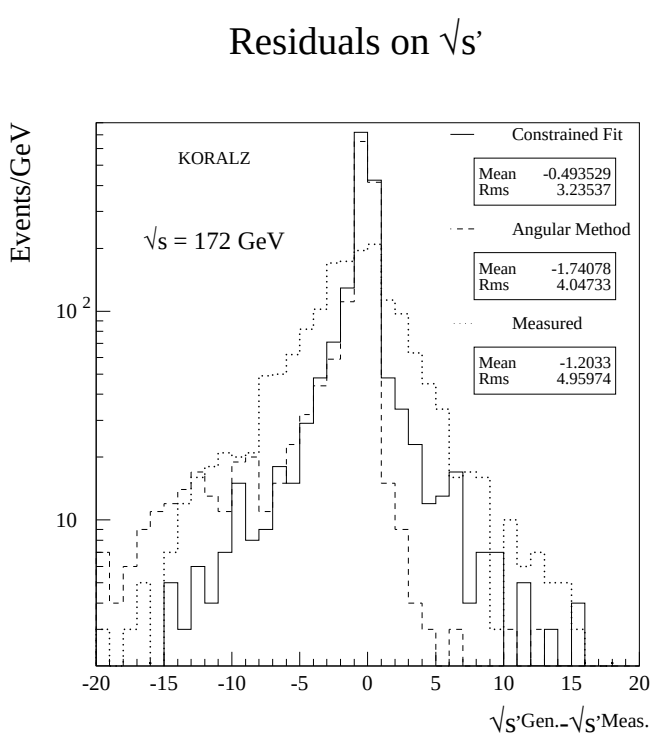

Figure 4: The residuals between the generated and fitted values of $\sqrt{s'}$ for three different methods: the constrained fit, the *angular method* and the measured values of the track parameters .

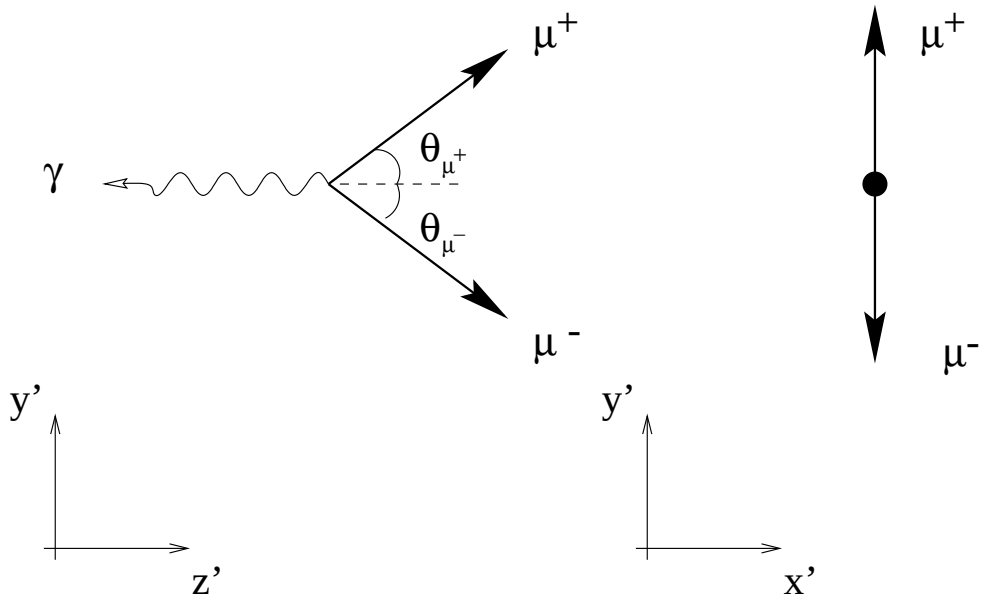

Figure 5: The topology of a radiative muon pair event when a photon is radiated collinear to the beam direction in an arbitrary set of Cartesian coordinates. As can be seen the event is planar.

5.1.2 Constrained Fitting

In the case of a $e^+e^- \to \mu^+\mu^-(\gamma)$ event the track parameters can be improved upon with 4–momentum constraints. Different constraints are needed for differing event topologies. These new track parameters provide an improved estimator of $\sqrt{s'}$ when used in Equation 2.

A χ^2 value was evaluated from the track parameters, the covariance matrix and a matrix representing the constraints. The fit starts with the measured track parameters and the χ^2 value is then minimised by iteration. Details of the algorithm are given in [11]. The constraints and implementation of the fits used in the analysis presented here are given below.

5.2 The Constrained Fit Applied to $e^+e^- \to \mu^+\mu^-(\gamma)$

The 4–momentum constraints on an $e^+e^- \to \mu^+\mu^-(\gamma)$ event are:

$$\mathbf{p}_{\mu^+} + \mathbf{p}_{\mu^-} + \mathbf{p}_\gamma = \mathbf{0}, \tag{6}$$

$$|\mathbf{p}_{\mu^+}| + |\mathbf{p}_{\mu^-}| + \mathrm{E}_\gamma = 2E_{\mathrm{BEAM}} = \sqrt{\mathrm{s}}, \tag{7}$$

where $\mathbf{p}_\gamma$ and E_γ are the momentum and energy of the photon respectively. The beam energy error was ~ 30 MeV [12] which was small compared to the errors on the momentum of the measured muon of $\mathcal{O}(\mathrm{GeV})$. Therefore, the value of E_{BEAM} was treated as a constant in the constrained fits.

There were five topologies of $e^+e^- \to \mu^+\mu^-(\gamma)$ events considered, when evaluating $\sqrt{s'}$, with a differing number of constraints, (nC where $n = 1, 3$ or 4), associated to each one. The topologies and constraints are outlined below.

- 4C: Seen γ
  If only one significant photon (~ 5 GeV) was radiated and observed in the detector, the 4-momentum conservation relations in Equations 6 and 7 were used as the constraints.

- 4C: No γ
  If there was no significant photon in the event, the 4-momentum conservation relations:

  $$\begin{aligned} \mathbf{p}_{\mu^+} + \mathbf{p}_{\mu^-} &= \mathbf{0}, \\ |\mathbf{p}_{\mu^+}| + |\mathbf{p}_{\mu^-}| &= \sqrt{\mathrm{s}}, \end{aligned}$$

  were used as constraints.

- 3C: Beampipe γ
  If there was one significant photon radiated in a direction collinear to the e^+ or e^- beam there were 3 constraints given by:

  $$\begin{aligned} \mathrm{p}^x_{\mu^+} + \mathrm{p}^x_{\mu^-} &= 0, \\ \mathrm{p}^y_{\mu^+} + \mathrm{p}^y_{\mu^-} &= 0, \\ |\mathbf{p}_{\mu^+}| + |\mathbf{p}_{\mu^-}| + \left|\mathrm{p}^z_{\mu^+} + \mathrm{p}^z_{\mu^-}\right| &= \sqrt{\mathrm{s}}, \end{aligned}$$

  where $\mathrm{p}^i_{\mu^\pm}$, $(i = x, y, z)$, is the $\mu^\pm$ momentum component in the x, y or z direction.

- 1C: Seen γ
  If there were two significant photons produced, one of which was detected and the other was not, there was one constraint given by:

$$|\mathbf{p}_{\mu^+}| + |\mathbf{p}_{\mu^-}| + \mathrm{E}_\gamma + |\mathbf{p}_{\mu^+} + \mathbf{p}_{\mu^-} + \mathbf{p}_\gamma| \;=\; \sqrt{\mathrm{s}}.$$

- 1C: Unseen γ
  If there was one significant photon produced in any direction, which went undetected, there was one constraint given by:

$$|\mathbf{p}_{\mu^+}| + |\mathbf{p}_{\mu^-}| + |\mathbf{p}_{\mu^+} + \mathbf{p}_{\mu^-}| \;=\; \sqrt{\mathrm{s}}.$$

The fits were applied successively using the scheme outlined in Figure 6[2]. The fits that involved a detected photon were only applied if $E_\gamma > 5$ GeV, the approximate $\sqrt{s'}$ resolution. If the 4C fit including a photon converged the computed value of $\sqrt{s'}$ along with the fitted track parameters were used. For the 4C fit, in which no photon was assumed, the value of $\sqrt{s'}$ was taken to be equal to $\sqrt{s}$. If any of the other fits converged and had a χ^2 probability, $P(\chi^2)$[3], was greater than 1% then the muon parameters from the fits were used to evaluate $\sqrt{s'}$. The approximate percentage of events for which a particular fit was used to evaluate $\sqrt{s'}$ is also given in Figure 6.

The distribution of $P(\chi^2)$ for simulation and data at 183 GeV is given in Figure 7. The peak observed at low values of $P(\chi^2)$ can be understood in terms of the fact that some properties of the events, which pass the $P(\chi^2) > 1\%$ cut, may not have satisfied all the assumptions in the fit. Examples of such discrepancies are:

- background topologies.
- topologies with two undetected photons.
- events with measured parameters in the tails of the residual distributions. The χ^2 minimisation assumes Gaussian errors on the measured parameters which do not fully describe the tails of the distribution (*i.e.* the muon momentum residual distribution is fitted with a double–Gaussian).

Despite these caveats, the constrained fit improves the $\sqrt{s'}$ resolution, as is discussed in Section 5.3.

In the case where all the kinematic fits either failed to converge or failed the cut on $P(\chi^2)$, the measured muon parameters were used. The *angular method* was not used on these events because the topologies that fail all the fits are those that are not described by the assumption of a single photon collinear to the beam (e.g. background events or those muon pair events with two undetected photons). If the value of $\sqrt{s'}$ was greater than $\sqrt{s}$, the value of $\sqrt{s'}$ was set equal to $\sqrt{s}$.

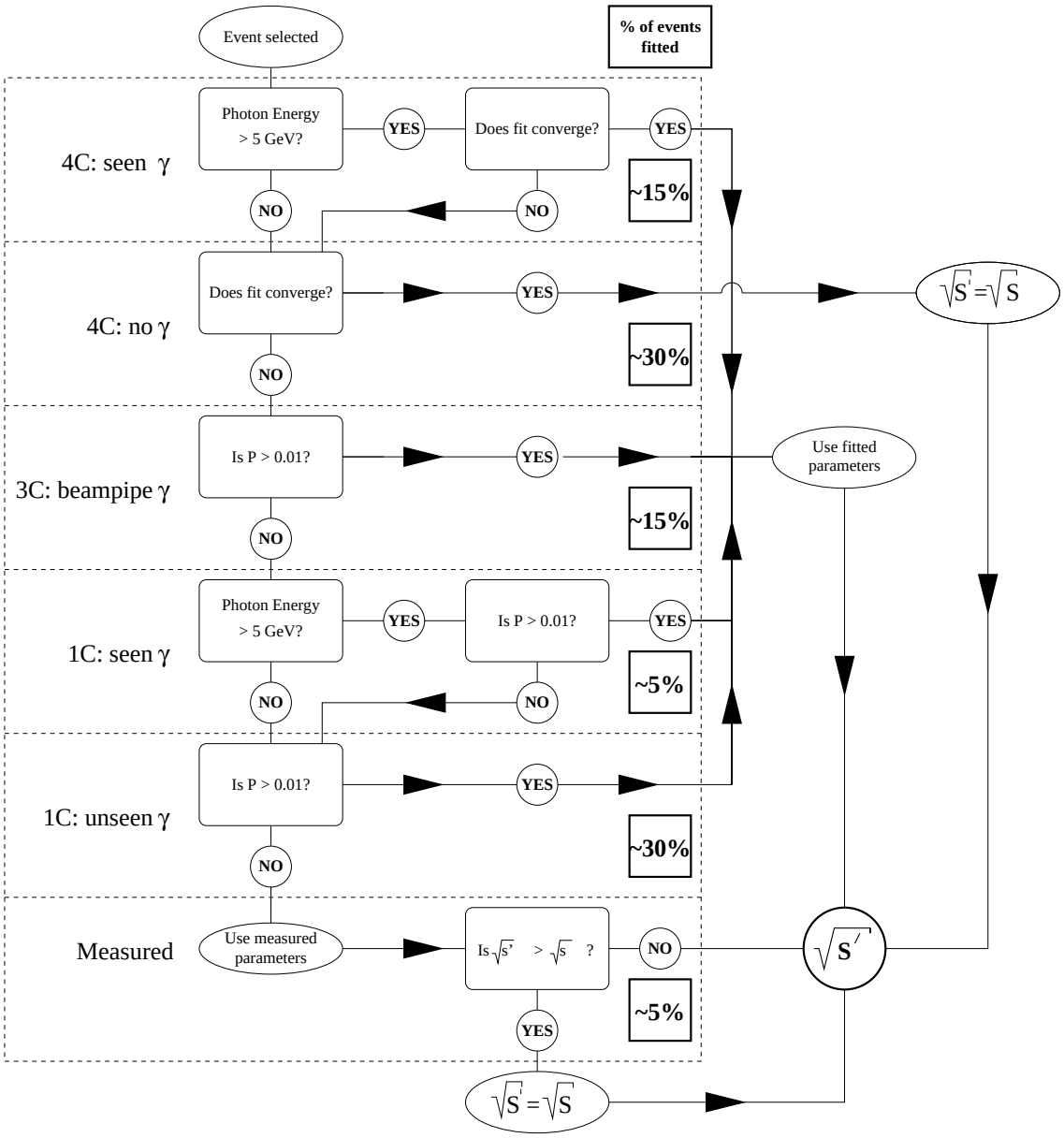

Figure 6: A flow diagram showing how the constrained fits were applied to a muon pair event that had passed the basic selection. The approximate percentage of events fitted at each stage are given in the bold boxes.

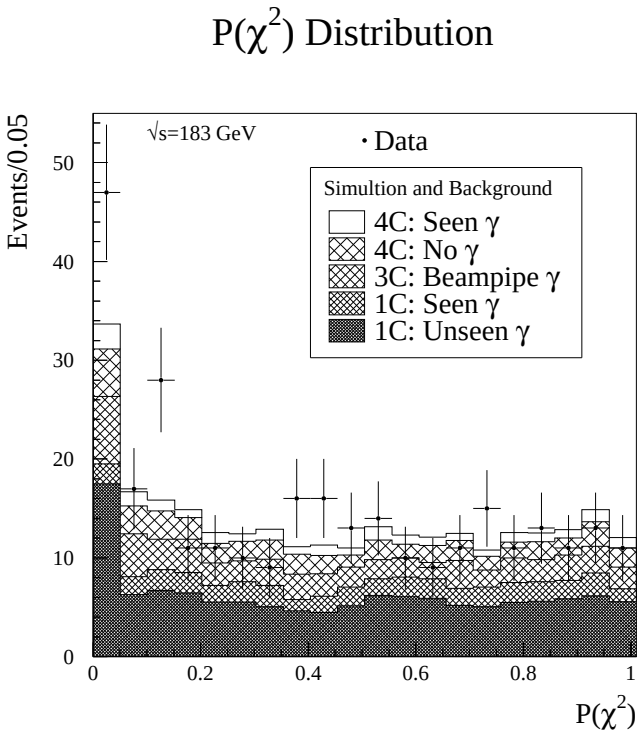

Figure 7: The $P(\chi^2)$ distribution for the simulation at $\sqrt{s} = 183$ GeV.

5.3 The $\sqrt{s'}$ Resolution

Some examples of the performance and resolution of the kinematic fit, compared to the *angular method*, will now be presented. The 172 GeV KORALZ simulation of $e^+e^- \to \mu^+\mu^-(\gamma)$ was used for all these comparisons.

The residuals between the generated value of $\sqrt{s'}$ and the values found from using either the constrained fit, the *angular method* or the track parameters, are given in Figure 4. The implementation of the constrained fit reduced the bias and the RMS of the distributions compared to the evaluation of $\sqrt{s'}$ using the angles. The large improvement from the use of the measured track parameters can also be seen; the RMS for the constrained fit distribution is $\sim \frac{2}{3}$ of that from the measured parameters.

The distributions of the generated, *angular method* and kinematic fitted values of $\sqrt{s'}/\sqrt{s}$, are given in Figure 8. The excess in the non–radiative part of the distribution evaluated using the *angular method* gave a larger impurity of events with $\sqrt{s'}/\sqrt{s} < 0.85$, which are reconstructed to values of $\sqrt{s'}/\sqrt{s} > 0.85$. This is referred to as the **ISR impurity**, the level of which is given in Section 6.

This is further illustrated in Figure 9 where the distributions of generated and measured values for the two methods are plotted against one another. There are three regions marked:

[2]The 4C fit with a seen photon was not used in the analysis performed by the Wuppertal group; the fitting procedure starts with the 4C fit in which no significant photon is assumed.

[3]The number of degrees of freedom used to evaluate $P(\chi^2)$ is equal to the number of constraints used in the fit.

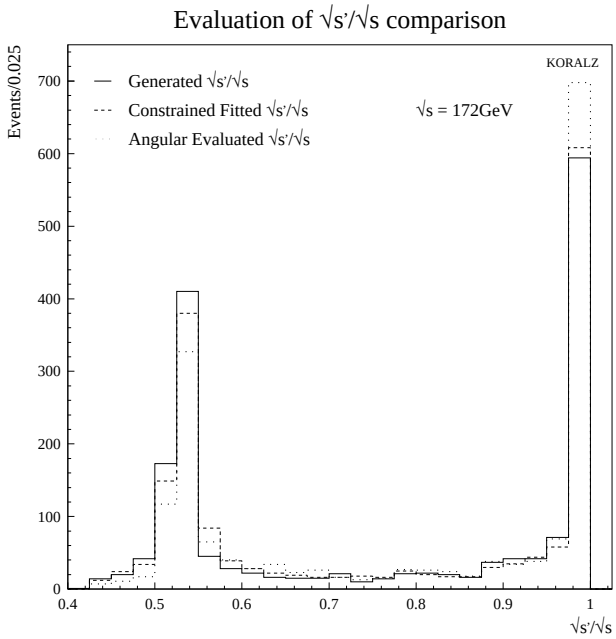

Figure 8: The distributions of $\sqrt{s'}/\sqrt{s}$ for the generated values, constrained fitted and *angular method* values.

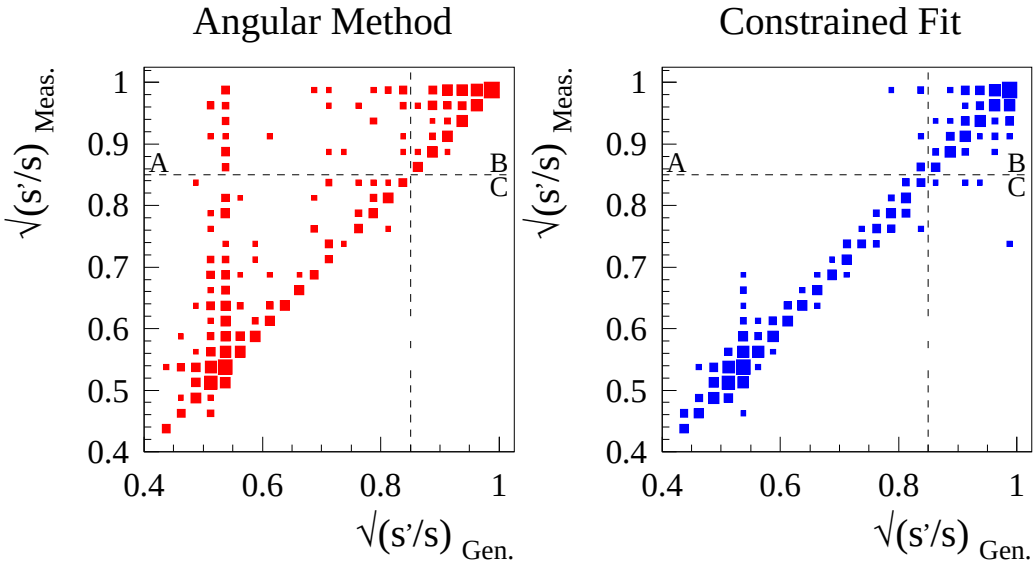

Figure 9: The distributions of $\sqrt{s'}/\sqrt{s}$ for the constrained fitted and *angular method* values plotted against the generated values.

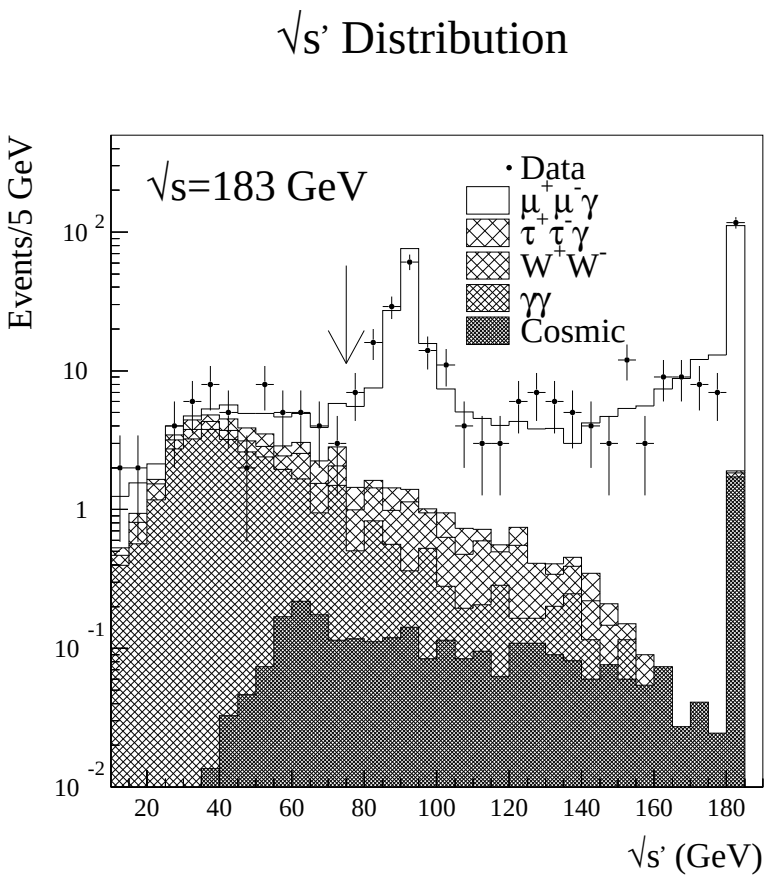

Figure 10: The distributions of $\sqrt{s'}$ for simulation and data at $\sqrt{s}$= 183 GeV. The arrow marks the cut on $\sqrt{s'}$ at 75 GeV.

- **Region A** in which the generated value of $\sqrt{s'}/\sqrt{s}$ was less than 0.85, but the measured value was greater than 0.85.
- **Region B** in which the both the generated and measured values of $\sqrt{s'}/\sqrt{s}$ were greater than 0.85.
- **Region C** in which the generated value of $\sqrt{s'}/\sqrt{s}$ was greater than 0.85,but the measured value was less than 0.85.

Events in region A are the ISR impurity in the non–radiative class of events and contaminate region B in the projection of the measured distribution. Region A is far less densely populated for the constrained fit distribution compared to that from the *angular method*. The number of events which have been incorrectly reconstructed into region C instead of region B was at a minimal level when the constrained fit was used, though the *angular method* yields no loss to this region.

5.4 The Removal of Background

The generally low momentum of particles arising from the physics background processes, lead to low values of $\sqrt{s'}$ for these events. Therefore, requiring a minimum value of

130 GeV		
Background	$\sqrt{s'}$>75 GeV	$\sqrt{s'}/\sqrt{s}$>0.85
Cosmic	$2.1 \pm 0.9\%$	$3.2 \pm 1.4\%$
$\tau^+\tau^-$	0.076 ± 0.031 pb	–
136 GeV		
Background	$\sqrt{s'}$>75 GeV	$\sqrt{s'}/\sqrt{s}$>0.85
Cosmic	$2.1 \pm 0.9\%$	$3.2 \pm 1.4\%$
$\tau^+\tau^-$	0.040 ± 0.019 pb	–
161 GeV		
Background	$\sqrt{s'}$>75 GeV	$\sqrt{s'}/\sqrt{s}$>0.85
Cosmic	$2.4 \pm 0.7\%$	$3.4 \pm 1.0\%$
$\tau^+\tau^-$	0.015 ± 0.008 pb	–
$\gamma\gamma$	0.082 ± 0.019 pb	–
W^+W^-	0.014 ± 0.010 pb	–
172 GeV		
Background	$\sqrt{s'}$>75 GeV	$\sqrt{s'}/\sqrt{s}$>0.85
Cosmic	2.3 ± 0.9	$2.2 \pm 1.0\%$
$\tau^+\tau^-$	0.033 ± 0.010 pb	–
$\gamma\gamma$	0.089 ± 0.021 pb	–
W^+W^-	0.069 ± 0.011 pb	–
183 GeV		
Background	$\sqrt{s'}$>75 GeV	$\sqrt{s'}/\sqrt{s}$>0.85
Cosmic	$0.78 \pm 0.13\%$	$0.97 \pm 0.16\%$
$\tau^+\tau^-$	0.054 ± 0.008 pb	–
$\gamma\gamma$	0.067 ± 0.008 pb	–
W^+W^-	0.100 ± 0.008 pb	–
189 GeV		
Background	$\sqrt{s'}$>75 GeV	$\sqrt{s'}/\sqrt{s}$>0.85
Cosmic	$0.46 \pm 0.04\%$	$0.46 \pm 0.04\%$
$\tau^+\tau^-$	0.066 ± 0.007 pb	–
$\gamma\gamma$	0.140 ± 0.022 pb	–
W^+W^-	0.155 ± 0.015 pb	–

Table 4: The percentage of cosmic events and the expected background cross sections for two–photon, $\tau^+\tau^-$ and W^+W^- processes at the different values of $\sqrt{s}$.

$\sqrt{s'}$ provided a good discriminator against the background.

The distribution of $\sqrt{s'}$ for events that passed all the selection criteria except that on $\sqrt{s'}$ at $\sqrt{s} = 183$ GeV, is given in Figure 10. A cut was placed at $\sqrt{s'} = 75$ GeV which excluded much of the background from two–photon events, $\tau^+\tau^-$ and fully leptonic W pair events.

Furthermore, the distribution of $\sqrt{s'}$ of the cosmic events can be seen to be spread both above and below 155 GeV ($\sqrt{s'}/\sqrt{s} \approx 0.85$ at 183 GeV) in Figure 10. If the *angular method* had been used this would all lie in the region of $\sqrt{s'}/\sqrt{s} > 0.85$; this would have increased the cosmic background in the region $\sqrt{s'}/\sqrt{s} > 0.85$ by approximately a factor of two compared to that when the constrained fit was used.

The contamination from the backgrounds that were expected at the different values of $\sqrt{s}$ are summarised in Table 4. The cosmic ray background is expressed as a percentage and the physics process backgrounds as a cross section in picobarns. The errors on these quantities are discussed in Section 7 along with the other systematic errors on $\sigma^{\mu\mu}$.

It was found that at 130 and 136 GeV, there was negligible contamination from two–photon events. This can be understood in terms the ISR photon spectrum at higher energy providing more events with a $\sqrt{s'} > 75$ GeV. In addition, there is an increase in the ratio of of two photon process, $\sigma^{\gamma\gamma}$, to $\sigma^{\mu\mu}$; the ratio of ratios, of two cross sections as $\sqrt{s}$ is increased from 130 GeV to 180 GeV is:

$$\frac{\sigma^{\mu\mu}(130 \text{ GeV})/\sigma^{\gamma\gamma}(130 \text{ GeV})}{\sigma^{\mu\mu}(180 \text{ GeV})/\sigma^{\gamma\gamma}(180 \text{ GeV})} \sim 2.$$

The number of cosmic ray background events is approximately proportional to the time taken to collect the data. The number of muon pair events is proportional to the total luminosity. Therefore, the greater the instantaneous luminosity the smaller fraction of cosmic background.This partially explains the variations in the level of background between years. However, there is also the fall of $\sigma^{\mu\mu}$ at higher energies and the statistical fluctuations in the number of cosmic events[4] to be considered.

5.5 $\sqrt{s'}/\sqrt{s}$ Distributions

The $\sqrt{s'}/\sqrt{s}$ distributions are given for the different years data in Figures 11 and 12. The data taken in 1995 and 1996 have been combined into one plot for each year and are given in Figure 11. The 183 GeV and 189 GeV data from 1997 and 1998 are presented separately in the two histograms in Figure 12.

The plots are normalised to the luminosity. The cross section for $e^+e^- \to \mu^+\mu^-(\gamma)$ was taken from ZFITTER version 6.11 [13] [5] to perform the normalisation. This accounted for any differences between the computed cross sections of KORALZ and ZFITTER.

The agreement can be seen to be good apart from at 183 GeV, where an excess of events is observed. This excess is reflected in the value of $\sigma^{\mu\mu}$ evaluated at 183 GeV which is discussed in the following section.

[4] Only 20 to 50 events were available, within the widened IP_z cuts, at each energy point to evaluate the cosmic background.

[5] All Standard Model expectations contained within this note are computed using this version of the ZFITTER program

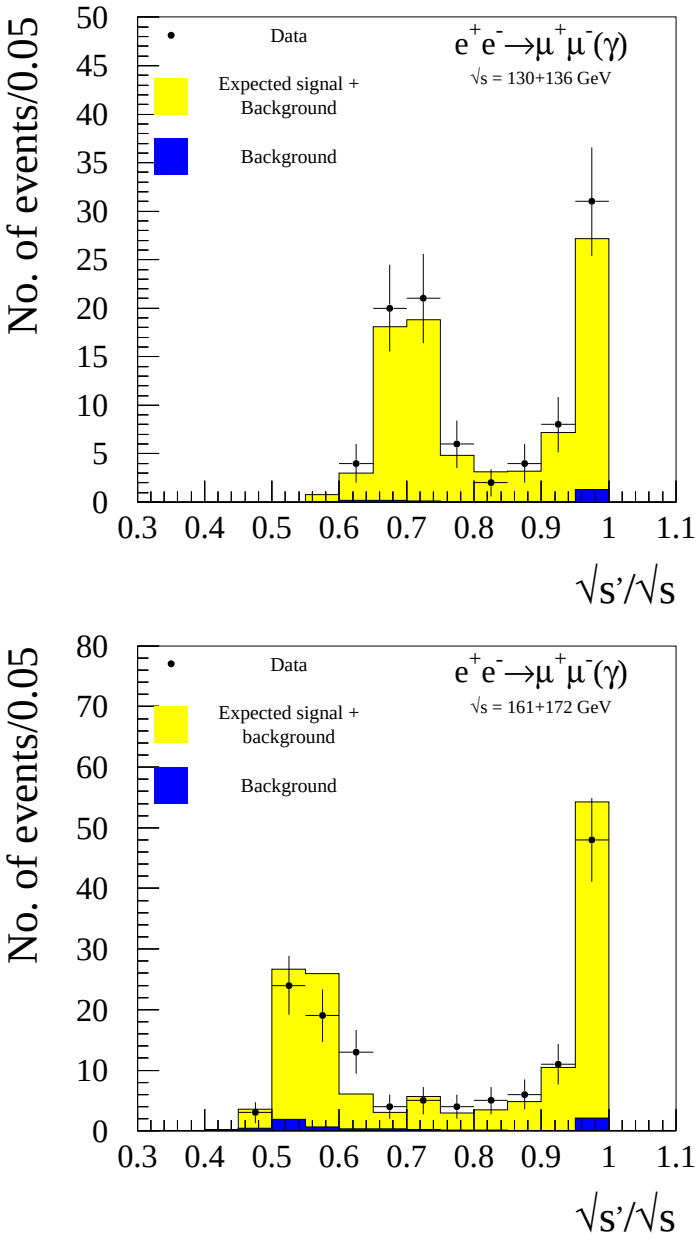

Figure 11: The $\sqrt{s'}/\sqrt{s}$ distributions for data and simulation for data taken in 1995 and 1996. The upper plot contains the data taken at 130 GeV and 136 GeV in 1995. The lower plot contains the data taken at 161 GeV and 172 GeV in 1996.

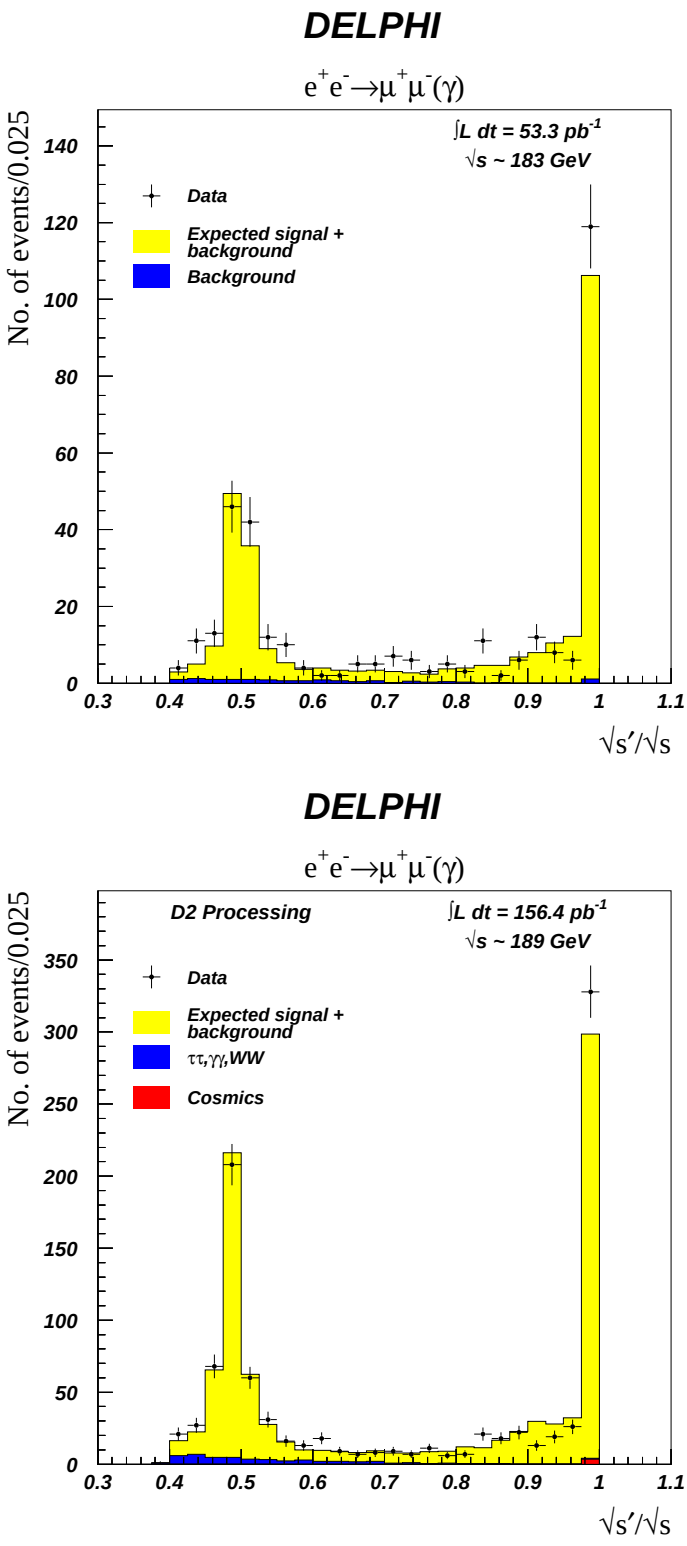

Figure 12: The $\sqrt{s'}/\sqrt{s}$ distributions for data and simulation for data taken in 1997 and 1998. The upper plot contains the data taken at 183 GeV in 1997. The lower plot contains the data taken at 189 GeV in 1998.

$\sqrt{s}$ (GeV)	**Efficiency**, η			**ISR impurity**
	$\sqrt{s'} > 75$GeV	$\sqrt{s'} > 0.85\sqrt{s}$	Correction	$\sqrt{s'} > 0.85\sqrt{s}$
130	$92.0 \pm 3.0\%$	$94.0 \pm 3.0\%$	-1%	$1.8 \pm 0.9\%$
136	$92.0 \pm 3.0\%$	$94.0 \pm 3.0\%$	-1%	$1.8 \pm 0.9\%$
161	$92.0 \pm 3.0\%$	$92.5 \pm 3.0\%$	-1%	$1.5 \pm 0.8\%$
172	$92.0 \pm 3.0\%$	$93.5 \pm 3.0\%$	-1%	$0.9 \pm 0.5\%$
183	$90.0 \pm 2.0\%$	$91.0 \pm 2.0\%$	-2%	$1.8 \pm 0.9\%$
189 (Simulation)	$91.8 \pm 3.0\%$	$94.5 \pm 3.0\%$	–	$2.2 \pm 1.1\%$
189 (Data)	$89.6 \pm 1.1\%$	$92.3 \pm 1.1\%$	–	–

Table 5: The efficiency at the different centre of mass energies. For 189 GeV the efficiency calculated from data is also given. The correction applied to the efficiency evaluated from the simulation is given in the third column. The fourth column contains the value of the ISR impurity evaluated at each energy point.

6 Determination of the Efficiency

For the data sets prior to 1998 the efficiency was determined using the simulation; this method is described in Section 6.1. The increased statistics available in 1998 allowed the efficiency to be determined from the data themselves. This is detailed in Section 6.2. This allowed a cross check to be performed with the efficiency calculated from the simulation and a subsequent reduction in the systematic error associated to the efficiency, which will be discussed in Section 7.

6.1 Selection Efficiency from Simulation

The selection efficiency is defined within the angular acceptance and was calculated from events generated with `KORALZ` which had then been passed through `DELSIM`. Additional smearings were applied to the simulation to yield better agreement with the data. These were performed for momentum and for the number of layers hit in the muon chamber system. These smearings are tuned at the different centre of mass energies and in angular bins. The momenta were smeared using a double Gaussian as at LEP1 [5].

The efficiency of selection, within the acceptance, is defined trivially as:

$$\eta = \frac{\text{Number of Selected Events}}{\text{Number of Generated Events}}. \tag{8}$$

6.2 Calculating the Efficiency using Data

The 1998 data was approximately three times larger than that of the previous year. This allowed the use of the data to evaluate the selection efficiency for the first time at LEP2. The selection efficiency within the acceptance, η, can be broken up into several components as follows:

$$\begin{aligned}\eta \;=\; & \eta(\text{Preselection}) \;\otimes\; \eta(\text{Trigger}) \;\otimes\; \eta(\sqrt{s'}) \;\otimes \\ & \eta^2(\text{Muon Identification}) \;\otimes\; \eta^2(\text{Track Reconstruction}) \;\otimes \\ & \eta(\text{Cuts}) \otimes \mathcal{C},\end{aligned}$$

where $\eta(\sqrt{s'})$ is the efficiency of the $\sqrt{s'}$ algorithm, $\eta(\text{Cuts})$ accounts for losses due to the sequential cuts applied and $\mathcal{C}$ is a correction factor for kinematical and topological considerations such as angular correlations. The data was used to calculate the single arm efficiency:

$$\eta(Single\ Arm) \;=\; \eta(\text{Track Reconstruction}) \;\otimes\; \eta(\text{Muon Identification}), \tag{9}$$

This gives a direct determination of the muon detection efficiency. Two different methods were used which are described elsewhere [5].

The component due to the efficiency for the trigger was evaluated using ~ 1000 dimuon events collected at 189 GeV. The value was found to be $(0.9994^{+0.0006}_{-0.0012})\%$[14]. The simulation was used to evaluate the other components.

6.3 The Efficiency Applied to the Data

The efficiencies determined from simulation were corrected by subtracting 1% or 2% from each value. It was observed at LEP1 that the efficiency extracted from the simulation was systematically lower, by approximately 1%, than that extracted from the data. These discrepancies were accounted for by the poor modelling of losses at the central plane and azimuthal sector boundaries of the TPC [15]. The efficiency from simulation was corrected by -1% for 1995 and 1996.

The determination of the efficiency from the 1998 data was found to be nearer 2% less than the simulation. Therefore the 1997 efficiency was corrected in retrospect by -2%. In 1998 the efficiency calculated from the data was used. The efficiencies determined, at the different centre–of–mass energies, from both simulation and data are given in Table 5.

6.4 The ISR impurity in the Non–Radiative Class

For events in the non-radiative class($\sqrt{s'} > 0.85\sqrt{s}$), the impurity due to the feed up of events with a $\sqrt{s'} < 0.85\sqrt{s}$ events has to be taken into account[6]. This was done using the simulation and was calculated according:

$$Purity, \mathcal{P} \;=\; 1 - \frac{N_{\sqrt{s'}/\sqrt{s}<0.85}}{N_{\text{selected}}} \tag{10}$$

where $N_{\sqrt{s'}/\sqrt{s}<0.85}$ is the number of events selected which are not in the non–radiative class at generator level and N_{selected} is the number of events selected in the non–radiative class.

The values of the ISR impurity at each energy point are given in Table 5.

[6]The migration of events 'down' is taken into account in the non radiative efficiency in the Oxford analysis. The Wuppertal analysis does not define the non–radiative efficiency in the same way; if the event is selected in the inclusive class it was considered to be selected. A scale factor was then applied to the non–radiative cross section that accounted for both feed up and feed down.

Energy (GeV)	Number of events for $\sigma^{\mu\mu}$		Number of events for $A_{\rm FB}^{\mu\mu}$			
	$\sqrt{s'} > 75$ GeV	$\sqrt{s'}/\sqrt{s} > 0.85$	$\sqrt{s'} > 75$ GeV		$\sqrt{s'}/\sqrt{s} > 0.85$	
			N_{fwd}	N_{bwd}	N_{fwd}	N_{bwd}
130.2	56	25	41	15	20	5
136.2	40	18	31	9	15	3
161.3	72	32	50	22	22	10
172.1	70	33	54	16	31	2
182.7	344	153	223	120	118	33
188.6	976	426	662	309	336	88

Table 6: The number of events selected at different $\sqrt{s}$ values. The numbers are divided into those selected in the two classes of $\sqrt{s'}$ and then into those in the forward and backward directions for the $A_{\rm FB}^{\mu\mu}$ measurement. The number of events used for the cross section and $A_{\rm FB}^{\mu\mu}$ measurements differ because events without associated luminosity are not used for the cross section analysis, and likesign events are not use in the $A_{\rm FB}^{\mu\mu}$ analysis.

Energy (GeV)	4π correction factors ($\eta_{4\pi}$)					
	$\sqrt{s'} > 75$GeV			$\sqrt{s'}/\sqrt{s} > 0.85$		
	Total	Forward	Backward	Total	Forward	Backward
130.3	1.153	1.151	1.157	1.103	1.119	1.016
136.3	1.163	1.159	1.172	1.102	1.118	1.024
161.2	1.195	1.182	1.220	1.100	1.114	1.045
172.1	1.211	1.194	1.246	1.100	1.113	1.050
182.7	1.225	1.206	1.265	1.098	1.112	1.050
189.0	1.233	1.212	1.275	1.098	1.110	1.052

Table 7: The correction factors to full solid angle on $\sigma^{\mu\mu}$ and $A_{\rm FB}^{\mu\mu}$ at different values of $\sqrt{s}$.

7 Results

The number of events selected at each energy point are given in Table 6. The number of events used in the cross section and forward–backward asymmetry analysis differed at some values of $\sqrt{s}$. The difference was due to an event being excluded from the $\sigma^{\mu\mu}$ analysis if there was no luminosity associated to the status period from which it came. An event with no luminosity was included in the $A_{\rm FB}^{\mu\mu}$ analysis, however any events in which both identified muons were of the same sign were excluded. For example, at 189 GeV there were no events selected from periods without associated luminosity and there were 3 likesign events.

Energy (GeV)	$\sigma^{\mu\mu} \pm \delta\sigma^{\mu\mu}_{stat} \pm \delta\sigma^{\mu\mu}_{syst}$(pb)			
	$\sqrt{s'} > 75$GeV		$\sqrt{s'}/\sqrt{s} > 0.85$	
	Data	ZFITTER	Data	ZFITTER
130.2	$24.3 \pm 3.2 \pm 0.8$	20.42	$9.7 \pm 1.9 \pm 0.4$	8.11
136.2	$17.0 \pm 2.6 \pm 0.6$	17.39	$6.6 \pm 1.6 \pm 0.3$	7.01
161.3	$9.3 \pm 1.1 \pm 0.3$	10.38	$3.6 \pm 0.7 \pm 0.1$	4.44
172.1	$8.9 \pm 1.1 \pm 0.3$	8.84	$3.6 \pm 0.7 \pm 0.1$	3.80
182.7	$8.93 \pm 0.47 \pm 0.21$	7.69	$3.58 \pm 0.28 \pm 0.09$	3.31
188.6	$7.31 \pm 0.23 \pm 0.10$	7.15	$3.02 \pm 0.15 \pm 0.05$	3.08

Table 8: The values of $\sigma^{\mu\mu}$ at different $\sqrt{s}$ compared to the ZFITTER predictions. The ZFITTER version used is 6.11.

7.1 Cross Section

The cross-section was evaluated using the formula:

$$\sigma^{\mu\mu} = \frac{(N_{sig} - N_{bkg})\Pi_{ISR}}{\epsilon_{sel}\mathcal{L}}\eta_{4\pi}, \tag{11}$$

where N_{sig} is the number of events observed, N_{bkg} is the number of background events expected, Π_{ISR} is the purity of the non–radiative class with respect to muon pairs with $\sqrt{s'}/\sqrt{s} < 0.85$, ϵ_{sel} is the selection efficiency, $\mathcal{L}$ is the integrated luminosity and $\eta_{4\pi}$ are correction factors to the full solid angle. The reasons for and calculation of the 4π correction factor to the full solid angle is discussed below.

7.1.1 The Correction Factors To The Full Solid Angle

The ZFITTER package calculates the values of $\sigma^{\mu\mu}$ and $A^{\mu\mu}_{\rm FB}$ as predicted by the Standard Model, including electroweak and QED corrections. These predictions can then be compared to the measured values. However, the program can only calculate observables for certain cuts on the final state phase space. There are three options:

- no cuts are placed,
- a cut on the maximum acollinearity and the minimum of the fermions' momenta,
- a cut on the minimum invariant mass of the fermion pair, $\sqrt{s'}$.

The two schemes with cuts also allow the angular acceptance of the anti–fermion to be defined.

The third choice was ideal for the analysis presented here, where cuts on $\sqrt{s'}$ and $\sqrt{s'}/\sqrt{s}$ were made. However, in this analysis cuts were placed on the polar angles of both identified muons. For the evaluation of the $\sigma^{\mu\mu}$ and $A^{\mu\mu}_{\rm FB}$ at the Z^0 resonance an angular cut on the μ^+ only was suitable because nearly all events were produced with small acollinearity (less then 10°). Therefore, a cut on one fermion to define the experimental angular acceptance was valid.

This was no longer a sensible assumption at LEP2 where events are produced frequently with considerably acollinearity. The μ^+ may have been within the experimental

Energy (GeV)	ISR⊗FSR Interference Correction Factors, $\eta_{ISR\otimes FSR}$			
	$\sqrt{s'} > 75$GeV		$\sqrt{s'}/\sqrt{s} > 0.85$	
	$\eta_{\sigma^{\mu\mu}}$	$\eta_{A_{\rm FB}^{\mu\mu}}$	$\eta_{\sigma^{\mu\mu}}$	$\eta_{A_{\rm FB}^{\mu\mu}}$
182.7	1.00062	1.00262	1.00378	1.00551
188.6	1.00037	1.00161	1.00229	1.00349

Table 9: ZFITTER predictions for the correction due ISR⊗FSR Interference. The corrections were applied to the 183 and 189 GeV results only. The correction to $A_{\rm FB}^{\mu\mu}$ is applied to the final number obtained, unlike the 4π correction factors which are applied to the forward and backward numbers of events.

acceptance while the μ^- could have been outside it. As the two muons must lie within the active tracking volume, so that the evaluation of the events $\sqrt{s'}$ could be made sensibly, the chosen angular acceptance had to be accounted for before a comparison to the Standard Model predictions from ZFITTER could be made.

The correction was made by generating large samples of muon pair events (100,000) at the different values of $\sqrt{s}$ with only a phase space cut in place at $\sqrt{s'}$=75 GeV. From these samples the fraction of events outside the experimental cuts on polar angle were evaluated. This was done for both $\sqrt{s'}$ regions over the whole acceptance and in the forward and backward hemispheres for the correction factors required for the $A_{\rm FB}^{\mu\mu}$ measurement.

The factors were evaluated using the DYMU3 [16] generator. The values of these factors are given in Table 7. The statistical error on these correction factors was 10^{-3}. The correction factors have also been calculated using KORALZ and agreement with DYMU3, within the statistical errors, was found.

7.1.2 Correction due to ISR⊗FSR Interference

The contributions due to the interference between initial state and final state radiation are not considered in the 4π correction factors calculated. These effects are greatest at small angles. ZFITTER incorporates such contributions up to $\mathcal{O}(\alpha)$ and their use is optional. This feature was used to calculate the correction factors to the observables. These are shown in Table 9, however the final corrections were only applied to the 183 and 189 GeV results.

7.2 The Systematic Error on $\sigma^{\mu\mu}$

The error on the measurement of $\sigma^{\mu\mu}$ has been dominated by statistics at all centre of mass energies during LEP2 running except in 1998 when the statistical and systematic errors magnitude are comparable. Therefore, the estimation of the systematic error has been conservative because their influence on the final accuracy of the measurements has been small. Furthermore, the cross checks between data and simulation, which would allow a reduction in the systematic error, have been difficult because of limited statistics at LEP2 apart from the data taken at 189 GeV. The individual contributions to the systematic error are outlined below.

The sources of systematic error and their relative values at 183 GeV and 189 GeVare summarised in Table 10.

Source	$\sqrt{s}$ (GeV)	$\sqrt{s'} > 75$GeV		$\sqrt{s'} > 0.85\sqrt{s}$	
		$\delta\sigma^{Rad.}$	δA_{FB}^{Rad}	$\delta\sigma^{NRad.}$	δA_{FB}^{NRad}
Efficiency	183	$\pm 2.2\%$	–	$\pm 2.2\%$	–
	189	$\pm 1.2\%$	–	$\pm 1.1\%$	–
Background	183	$\pm 0.3\%$	$\pm 0.6\%$	$\pm 0.2\%$	$\pm 0.5\%$
	189	$\pm 0.4\%$	$\pm 0.6\%$	$\pm 0.1\%$	$\pm 0.2\%$
Luminosity	183	$\pm 0.6\%$	–	$\pm 0.6\%$	–
	189	$\pm 0.6\%$	–	$\pm 0.6\%$	–
ISR Impurity	183	–	–	$\pm 0.9\%$	$\pm 0.5\%$
	189	–	–	$\pm 1.1\%$	$\pm 0.5\%$
Correction Factors	183	$\pm 0.03\%$	$\pm 0.13\%$	$\pm 0.19\%$	$\pm 0.28\%$
	189	$\pm 0.02\%$	$\pm 0.08\%$	$\pm 0.11\%$	$\pm 0.17\%$
Total	183	$\pm 2.4\%$	$\pm 0.6\%$	$\pm 2.5\%$	$\pm 0.8\%$
	189	$\pm 1.4\%$	$\pm 0.6\%$	$\pm 1.7\%$	$\pm 0.6\%$

Table 10: The sources and associated values of systematic errors for 183 and 189 GeV. The slashed boxes mean that the source is not a contributing systematic to the measurement.

7.2.1 Selection Efficiency

The error on the efficiency coming from simulation statistics alone would be less than 1%. However, because of the known problems from LEP1 and the evaluation of the efficiency from the data in 1998, an error of 2% or 3% was assigned to the data sets where the efficiency was determined from the simulation alone. A 2% error was assigned to the efficiency at 183 GeV where differences between data and simulation arising in the muon identification and momentum resolution had been corrected. A more conservative error of 3% was assigned to the efficiency to the 1995 and 1996 data sets. For 189 GeV the statistical error from the determination the efficiency from data was used.

7.2.2 ISR Purity

The error on Π_{ISR} was again inflated from the value arising from the simulation statistics alone for similar reasons to those quoted above for the selection efficiency. An error of:

$$\delta\Pi_{ISR} = \frac{1}{2}(1 - \Pi_{ISR}), \tag{12}$$

was chosen to prevent the error increasing the purity to an unphysical value greater than one.

7.2.3 Background processes

The error associated with the background physics processes was taken from the simulation statistics alone. The cosmic ray background error came from the statistical uncertainty on the number of events used to extrapolate into the allowed $IP_{R\phi}$ region after tight IP_Z cuts had been made.

Energy (GeV)	$A_{\rm FB}^{\mu\mu} \pm \delta A_{\rm FB}^{\mu\mu}(stat) \pm \delta A_{\rm FB}^{\mu\mu}(syst)$			
	$\sqrt{s'} > 75$GeV		$\sqrt{s'}/\sqrt{s} > 0.85$	
	Data	ZFITTER	Data	ZFITTER
130.2	$0.452 \pm 0.119 \pm 0.004$	0.329	$0.669 \pm 0.152 \pm 0.009$	0.714
136.2	$0.558 \pm 0.131 \pm 0.005$	0.330	$0.741 \pm 0.166 \pm 0.010$	0.697
161.3	$0.389 \pm 0.109 \pm 0.003$	0.320	$0.425 \pm 0.161 \pm 0.005$	0.626
172.1	$0.547 \pm 0.100 \pm 0.006$	0.319	$0.904 \pm 0.074 \pm 0.010$	0.609
182.7	$0.289 \pm 0.052 \pm 0.002$	0.317	$0.565 \pm 0.066 \pm 0.004$	0.594
188.6	$0.361 \pm 0.030 \pm 0.002$	0.316	$0.600 \pm 0.039 \pm 0.003$	0.588

Table 11: The values of $A_{\rm FB}^{\mu\mu}$ at different $\sqrt{s}$ compared to the ZFITTER predictions. The ZFITTER version used is 6.11.

7.2.4 Luminosity

There are three sources of error on the luminosity evaluation:

- The statistical error coming from the number of Bhabha events used to evaluated the luminosity.
- The systematic error of 0.5% to 1.0% in the experimental evaluation, coming from the uncertainty in the STIC acceptance, the error in the position of the beam spot and any inaccuracies in the simulation of STIC detector.
- There is 0.25% systematic error in the theoretical calculation of the Bhabha scattering cross section.

The statistical and systematic errors on the luminosity are given in Table 1.

7.3 The Forward–Backward Asymmetry

The value of $A_{\rm FB}^{\mu\mu}$ was evaluated using the counting method:

$$A_{\rm FB}^{\mu\mu} = \frac{N^{fwd} - N^{bwd}}{N^{fwd} + N^{bwd}} \tag{13}$$

where N^{fwd} and N^{bwd} are the number of μ^- with $\cos\theta > 0$ or $\cos\theta < 0$ respectively.

The numbers in the forward and backward hemispheres were calculated with the formula:

$$N^x = (N^x_{obs} - N^x_{bkg})\eta^x_{4\pi}, \tag{14}$$

where x is either forward (fwd) or backward (bwd). The efficiency for selection was considered to be symmetric about $\cos\theta = 0$. Studies of $e^+e^- \to \mu^+\mu^-$ events at the Z^0 resonance [4] showed that the detector asymmetry was consistent with zero.

The statistical error on the $A_{\rm FB}^{\mu\mu}$ is given by:

$$\delta A_{\rm FB}^{\mu\mu} = \sqrt{\frac{1 - A_{\rm FB}^{\mu\mu 2}}{N_{obs}}}, \tag{15}$$

which can be derived from the binomial error on the number of events in one hemisphere.

7.4 The Systematic Error on $A_{\rm FB}^{\mu\mu}$

The systematic errors from the efficiency and the luminosity no longer contribute to the systematic error as these quantities are factored out in the division. The sources and relative values of systematic error for 183 and 189 GeV are summarised in Table 10.

7.4.1 Background Processes

The absolute level and the asymmetry of the background contributes towards the systematic error. The $\tau^+\tau^-$ and $\mathrm{W}^+\mathrm{W}^-$ events lead to a positive asymmetry in the background angular distributions for $\sqrt{s'} > 75$ GeV. This was the dominant systematic error for the $\sqrt{s'} > 75$ GeV class at all energies and for the $\sqrt{s'}/\sqrt{s} > 0.85$ class for energies less than 183 GeV.

7.4.2 ISR Purity

There was a possible systematic error from the Π_{ISR} distorting the value of $A_{\rm FB}^{\mu\mu}$ in the non–radiative class of events. This was evaluated from the simulation and was consistent with unity to within 0.5% of the $A_{\rm FB}$ in all cases which was taken to be the systematic error. This was the dominant error in the non–radiative class at 183 GeV and 189 GeV.

7.4.3 Likesign Events

A likesign event is one in which the two muons have been assigned the same charge. Likesign events arise from a mismeasurements of a track's curvature. Therefore, likesign events are more likely to occur in events with one track in the forward regions, where the transverse momentum is least well measured. The percentage of likesign events in the data at 183 GeV was $0.6 \pm 0.4\%$ though only $0.055 \pm 0.027\%$ were expected from the simulation. If both tracks in an event were assigned the incorrect charge this would lead to a bias in the evaluation of $A_{\rm FB}^{\mu\mu}$. However, from the single arm charge misassignment rate, and taking the probability of misassignment in both arms to be uncorrelated, the probability of both tracks being assigned the wrong charge is $\sim 10^{-3}\%$.

7.4.4 Correction Factors

The correction of the observable to 4π was performed using generators that do not incorporate initial and final state interference. $\mathcal{O}(\alpha)$ interference contributions are evaluated using `ZFITTER`. A relative systematic error associated with missing higher orders was applied. This was taken to be half of the correction.

$$\delta\eta_{ISR\otimes FSR} = \frac{1}{2}\eta_{ISR\otimes FSR}$$

7.5 Differential Cross Section

For data taken at 183 GeV and 189 GeV there were enough statistics to produce meaningful differential distributions for the non radiative samples. The angular distributions are given for data and simulation in Figure 7.5. The simulation is scaled to account for the differences in detection efficiency between data and simulation. Table 12 gives the differential cross sections, calculated in 10 bins of $\cos\theta$, for the two energies compared with

the Standard Model expectation. The differential cross sections are found to be in good agreement. Efficiencies were calculated bin by bin using simulation and then corrected as before.

7.6 Systematics on the Differential Cross Section

Systematic errors are dominated by the uncertainties on the efficiency and ISR impurity. The relative errors are similar to those expressed for the non radiative cross section in Table 10. The total absolute values for the bin by bin systematics are shown in Table 12.

7.6.1 Selection Efficiency

The efficiency contribution consists of an uncorrelated part, associated with the bin by bin statistical error on the efficiency from simulation and a fully correlated part[7] which arises from the uncertainty on the global selection efficiency. The latter is the dominant contribution.

7.6.2 ISR Purity

The differential cross sections are distorted by the ISR impurity. A systematic error associated to this was assigned to the differential cross section in each bin. The distribution of this contamination was assumed flat in θ so this contribution is fully correlated bin by bin.

7.6.3 Luminosity

The uncertainty on the luminosity measurement gave a fully correlated error on each bin.

7.6.4 Background

The only background contamination is from cosmic rays. It gives a negligible, partially correlated, contribution to the systematic error in each bin The correlation arises from the shape of the distribution which is peaked at $\cos\theta = 0$.

7.7 Comparison with the Standard Model

The cross section results for the 6 energy points are given in Table 8 and those for the forward–backward asymmetry are given in Table 11. The deviation from the Standard Model for the four different measurements at the 6 energy points are given in Figure 7.7. Where,

$$\text{Pull} = \frac{\text{X}_{\text{Measured}} - \text{X}_{\text{ZFITTER}}}{\delta\text{X}}$$

X represents the quantity measured, σ or A_{fb}, and δX is the measured error on this quantity.

There were two significant disagreements with the Standard Model predictions: the non–radiative $A_{\text{FB}}^{\mu\mu}$ at 172 GeV and the $\sqrt{s'} > 75$ GeV $\sigma^{\mu\mu}$ at 183 GeV.

[7] The fully correlated errors provide an equal relative contribution to the systematic error in each bin.

$\sqrt{s} \sim$ 183 GeV		
$\cos\theta$	SM (pb)	$d\sigma/d\cos\theta$ (pb)
[-0.94,-0.80]	0.478	$0.000 \pm 0.178 \pm 0.013$
[-0.80,-0.60]	0.486	$0.514 \pm 0.230 \pm 0.013$
[-0.60,-0.40]	0.576	$0.989 \pm 0.313 \pm 0.024$
[-0.40,-0.20]	0.761	$0.972 \pm 0.307 \pm 0.023$
[-0.20, 0.00]	1.045	$1.298 \pm 0.360 \pm 0.032$
[0.00, 0.20]	1.428	$1.591 \pm 0.398 \pm 0.039$
[0.20, 0.40]	1.913	$1.605 \pm 0.401 \pm 0.039$
[0.40, 0.60]	2.503	$3.377 \pm 0.579 \pm 0.081$
[0.60, 0.80]	3.206	$2.466 \pm 0.503 \pm 0.061$
[0.80, 0.94]	4.078	$4.978 \pm 0.841 \pm 0.119$

$\sqrt{s} \sim$ 189 GeV		
$\cos\theta$	SM (pb)	$d\sigma/d\cos\theta$ (pb)
[-0.97,-0.80]	0.465	$0.495 \pm 0.143 \pm 0.008$
[-0.80,-0.60]	0.467	$0.478 \pm 0.128 \pm 0.008$
[-0.60,-0.40]	0.546	$0.448 \pm 0.120 \pm 0.007$
[-0.40,-0.20]	0.713	$0.391 \pm 0.113 \pm 0.006$
[-0.20, 0.00]	0.971	$1.287 \pm 0.212 \pm 0.021$
[0.00, 0.20]	1.322	$1.129 \pm 0.197 \pm 0.018$
[0.20, 0.40]	1.769	$1.908 \pm 0.248 \pm 0.029$
[0.40, 0.60]	2.315	$2.445 \pm 0.290 \pm 0.039$
[0.60, 0.80]	2.968	$2.927 \pm 0.325 \pm 0.048$
[0.80, 0.97]	3.780	$3.986 \pm 0.413 \pm 0.065$

Table 12: The differential cross–sections for $\mu^+\mu^-$ and $\tau^+\tau^-$ final states at centre of mass energies of $\sim$ 183 and 189 GeV. The errors shown are the statistical and systematic components. For 183 GeV , where there were no events in the most backward bin, the statistical error has been taken to be the error on the expected number of events. Its systematic component is taken as the value of the systematic uncertainty in the neighbouring bin. The Standard Model expectations (SM) were computed with the ZFITTER.

The number of non–radiative events with $\cos\theta_{\mu^-} < 0$ is 2 at 172 GeV. This gave a value of the asymmetry which was $+4\sigma$ above the Standard Model prediction of 0.606. However, with only 2 events in one hemisphere the assumption of large statistics in the derivation of the $A_{\rm FB}^{\mu\mu}$ error is no longer valid. An alternative method was therefore used to evaluate the statistical error using Poisson statistics.

The mean values of a Poisson distribution at which the upper or lower limit of the 1σ confidence region is 2 were used to evaluate $A_{\rm FB}^{\mu\mu}$. The difference with the measured value of $A_{\rm FB}^{\mu\mu}$ was then taken to be the error. The errors, which are now asymmetric, are $+0.076$ and -0.113. With these errors the observed $A_{\rm FB}^{\mu\mu}$ is in fact $+3\sigma$ above the Standard Model prediction. Therefore, even though the result was unlikely it was not as improbable as the first error suggests.

The cross section at 183 GeV was $\sim 2\sigma$ high, though the values of $A_{\rm FB}^{\mu\mu}$ were in good agreement. There was no obvious discrepancy in any particular region of the $\sqrt{s'}$ or angular distributions. Further checks were made on the cosmic background, the seen photon distribution and muon identification by changing the selection criteria though no significant differences were observed. Therefore, the high cross section was concluded to be a statistical fluctuation.

8 Conclusion

The $e^+e^- \to \mu^+\mu^-(\gamma)$ cross–sections and forward–backward asymmetries have been determined at all LEP2 centre–of–mass energies from 1995 to 1998. In addition, the differential cross–sections have been given for the high statistic data sets taken in 1997 and 1999. The cross–sections have been determined in two ranges of the effective invariant mass of the muon pair: $\sqrt{s'}/\sqrt{s} > 0.85$ and $\sqrt{s'} > 75$ GeV. The determination of $\sqrt{s'}$ was performed using a constrained fitting method; this method improved the $\sqrt{s'}$ resolution and background rejection in the $\sqrt{s'}/\sqrt{s} > 0.85$ range. This is the range that is most sensitive to possible new physics contributions to the process.

The results presented in this note, along with those for other $e^+e^- \to f\bar{f}$ processes, have been used to determine limits on the parameters of several new physics processes: contact interactions, R–parity violating supersymmetry, additional neutral gauge bosons and gravity interactions in extra dimensions. These limits are presented in [1]and [2].

The authors would like to thank the other members of team 2 – John Holt, Peter Renton and Guy Wilkinson – for their input into the production of these results.

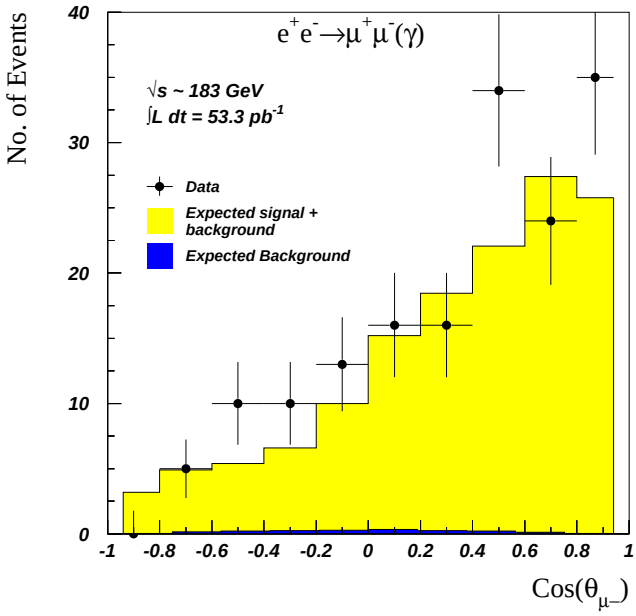

(a)

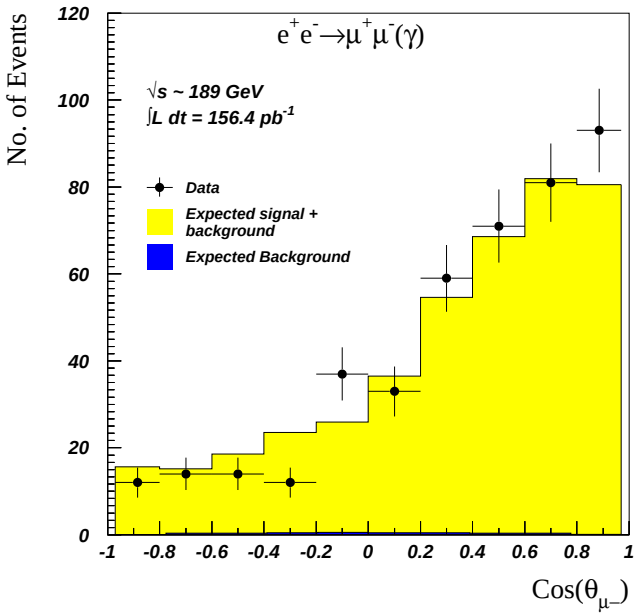

(b)

Figure 13: Angular Distribution for non-radiative muons compared with KORALZ simulation for (a) 183 and (b) 189 GeV . The simulation has been corrected by -2% for 183GeV . At 189GeV the simulation has been corrected for by the difference in the single arm muon efficiencies for data and simulation. This is described in [5].

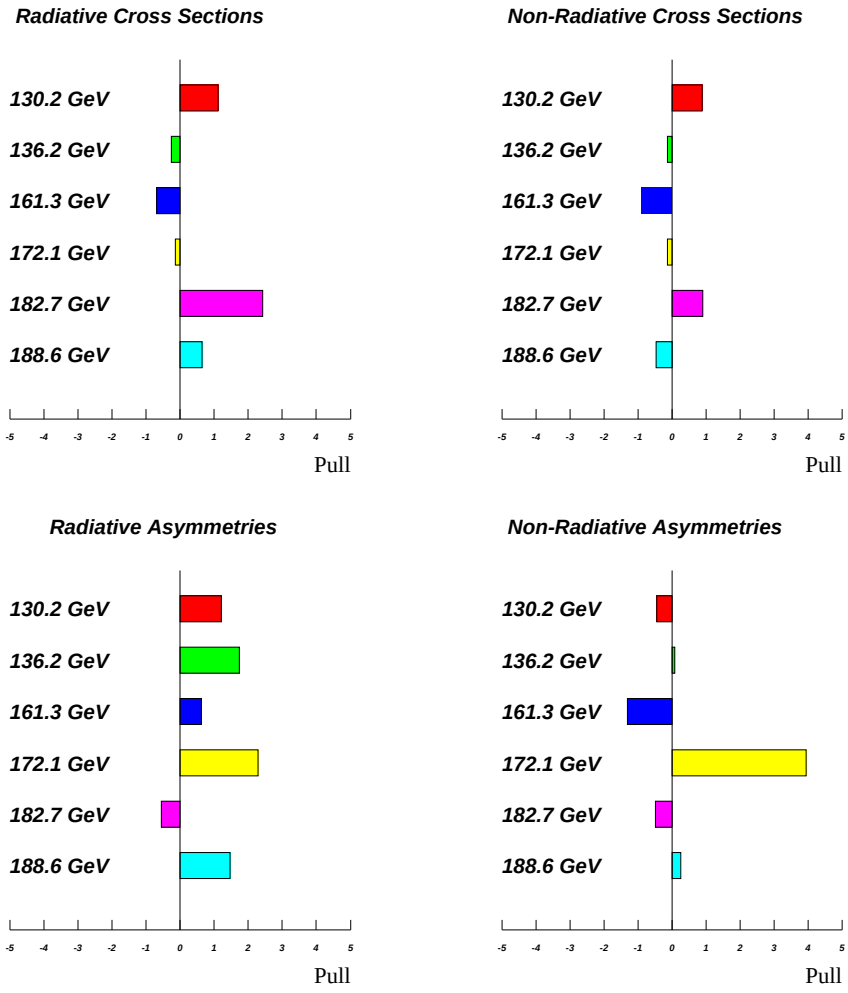

Figure 14: Pull plots for all energy points and measurements considered.

References

[1] DELPHI Collaboration (P. Abreu *et al*). Measurement and Interpretation of Fermion-Pair Production at LEP energies from 130 to 172 GeV. *CERN-EP/99-05 Submitted Eur. Phys. J. C. (1999).*

[2] A. Behrmann *et al* . Results on Fermion-Pair Production at LEP running near 183 GeV and 189 GeV. *DELPHI 99-135 HEP'99 CONF 322 (1999).*

[3] OPAL Collaboration (G. Abbiendi *et al*). Search for an Indirect Signal for the Gravity Interaction in Extra Dimensions Using Muon, Tau and Photon Pairs at $\sqrt{s'}$= 183 and 189 GeVat LEP. *OPAL Physics Note PN381 (1999).*

[4] R. Lindner, G.Wilkinson. DELPHI Muon Pair Cross-Section and Forward-Backward Asymmetry Analyses for the 1993 LEP Scan. *DELPHI 96-3 PHYS 587 (1996).*

[5] A. Behrmann, G.W. Morton. Determination of the Muon ID and Track Reconstruction Efficiencies using Data collected in 1998. *DELPHI 2000-002 PHYS 845 (2000).*

[6] S. Jadach, B.F.L. Ward, Z. Was. Koralz version 4.0. *Comput. Phys. Commun.* **79** *503 (1994).*

[7] F.A. Berends, R. Kleiss, R. Pittau. `EXCALIBUR`: A Monte Carlo Program to Evaluate all Four Fermion Processes at LEP-200 and Beyond. *Comput. Phys. Commun.* **85** *437-452 (1995).*

[8] F.A. Berends *et al* . Monte Carlo Simulation of Two Photon Processes. *Comput. Phys. Commun.* **40** *271 (1986).*

[9] DELPHI Collaboration (P. Abreu *et al*). Cross Sections and Leptonic Forward–Backward Asymmetries from the Z Running of LEP. *To be submitted to Eur. Phys. J. C. (1998).*

[10] P.B. Renton. Private Communication.

[11] N. Kjær, R. Möller. Reconstruction of Invariant Masses in Multi-Jet Events. *DELPHI 91-17 PHYS 88 (1991).*

[12] LEP Energy Working Group (A. Blondel *et al*). Evaluation of the LEP centre–of–mass energy above the W–pair production threshold. *CERN–EP/98-191 (1998) to be submitted to Eur. Phys J. C.*

[13] D. Bardin *et al* . `ZFITTER` v6.21 A Semi–analytical Program for Fermion Pair Production in e^+e^- Annihilation. *DESY 99-070, HEP-PH/9908433 (1999).*

[14] V. Canale. Private Communication.

[15] T. Burgsmüller. *Untersuchung der Myon-Paarprodukduktion bei Energien auf und oberhalb der Z–Resonanz.* PhD thesis, University of Wuppertal *(1998)*.

[16] J.E.Campagne, R.Zitoun. Electromagnetic Radiative Corrections at LEP - SLC Energies for Experimentalists. *Z. Phys* **C43** *469 (1989)*.